

# Time-Bandwidth Product of the Photonic Time-Stretched Analog-to-Digital Converter

Yan Han and Bahram Jalali, *Senior Member, IEEE*

**Abstract**—The time-bandwidth product of the photonic time-stretched system is modeled in terms of physical system parameters. Using the time-bandwidth product as figure-of-merit, the performances of optical double-sideband and single-sideband (SSB) intensity modulation are compared, and optical SSB intensity modulation is identified as a potential solution to extend the system's time-bandwidth product. An SSB-modulated time-stretched system is theoretically analyzed and experimentally demonstrated. As an important practical consideration, the analytical model relating the system performance to the phase and amplitude mismatches in the SSB modulator is presented. The results show that the system is tolerant to such unavoidable mismatches. Experiments using commercially available components suggest that the dispersion-induced power penalty can be kept below 2.5 dB over 4–20 GHz bandwidth for any stretch factor. Additional experiments demonstrating 120-GSamples/s real-time digitization of a 20-GHz SSB-modulated signal are also reported.

**Index Terms**—Analog-to-digital conversion (ADC), fiber optics, microwave photonics, optical signal processing, time stretch.

## I. INTRODUCTION

A SAMPLING oscilloscope is an effective tool for capturing ultrafast electrical signals that are repetitive in time. However, such measurements only provide average information about the signal. In contrast, real-time capture of ultrafast electrical signals is a difficult problem that challenges the state-of-the-art in analog-to-digital converters (ADCs). To extend the performance of electronic ADCs, the time-stretched analog-to-digital converter (TS-ADC) concept, shown in Fig. 1, has been proposed [1]. A single-channel time-stretched unit permits the capture of an ultrafast time-limited (transient) signal with an ADC that lacks sufficient sampling rate and input bandwidth. A multichannel TS-ADC will be able to capture continuous-time signals, as discussed elsewhere [2]. A multichannel time-stretched ADC is superior to a conventional ADC array based on the sample-interleaved architecture [3]. Among the advantages are the following. The signal bandwidth is reduced in the time-stretched system while unchanged in the sample-interleaved array. Hence, the time-stretched system not only increases the sampling rate, but also is more immune to sample-clock jitter. This paper is concerned with properties of the single-channel system and, hence, the capture of time-lim-

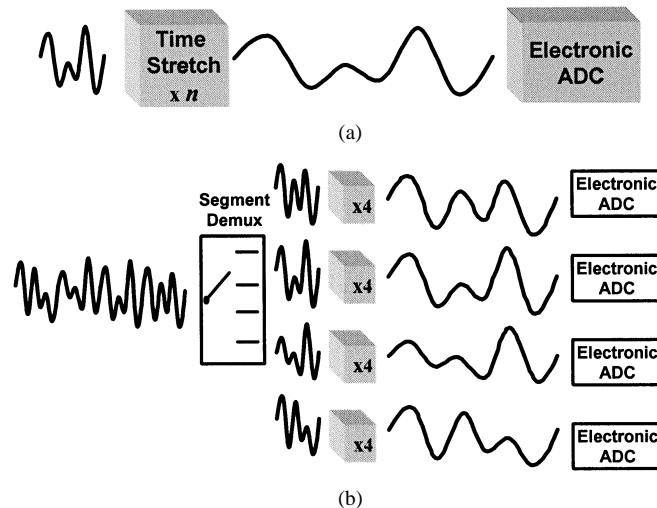


Fig. 1. Conceptual block diagram for: (a) single-channel and (b) multichannel TS-ADC. The single-channel TS-ADC can capture the transient signal, while the multichannel TS-ADC is able to capture the continuous signal.

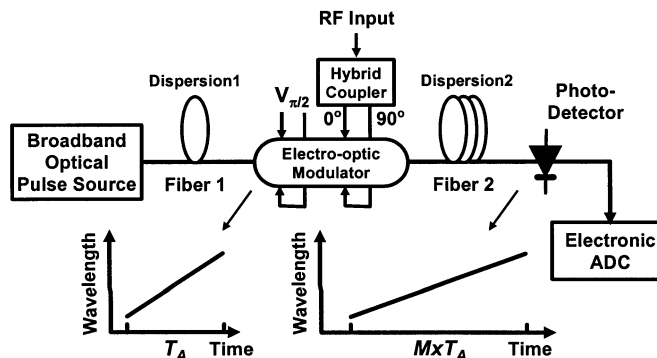


Fig. 2. Block diagram of the photonic time-stretched ADC. Time-to-wavelength plots are used to illustrate the stretch process.  $T_A$  denotes the input time aperture. Optical SSB intensity modulation is shown.

ited signals. However, the results and conclusions also apply to the continuous-time TS-ADC system.

A practical method for implementing the time-stretched function is to use the photonic technique shown in Fig. 2 [4]. A linearly chirped optical pulse is generated by propagating (in a fiber) the broad-band (nearly transform limited) pulses generated by a supercontinuum source [5]. The electrical input signal modulates the intensity of the chirped optical carrier in an electrooptic modulator. The envelope is subsequently

Manuscript received January 25, 2003; revised March 22, 2003. This work was supported by the Defense Advanced Research Project Agency under the Photonic Analog-to-Digital Converter Program.

The authors are with the Optoelectronic Circuits and Systems Laboratory, Department of Electrical Engineering, University of California at Los Angeles, Los Angeles, CA 90095 USA (e-mail: yhan@ee.ucla.edu).

Digital Object Identifier 10.1109/TMTT.2003.814313

stretched in a second spool of fiber before photodetection and digitization by a moderate-speed electronic ADC. Based on this method, 130-GSample/s digitization of time-limited signals has recently been demonstrated [4]. The input time-aperture  $T_A$  and bandwidth are two fundamental performance parameters of the TS-ADC system. The input time aperture is the duration of the chirped optical pulse at the modulator input and represents the maximum length of the RF signal that can be captured (Fig. 2). It has been shown that the dispersion penalty in the second fiber will limit the maximum system bandwidth, when the conventional optical double-sideband (DSB) intensity modulation is used [6]. As will be shown in Section II, the bandwidth can be improved, but only at the expense of the time aperture. Consequently, neither time aperture, nor bandwidth itself is a good metric to evaluate the performance of the TS-ADC. The product of these two parameters is found to be a more suitable metric and is, therefore, used throughout this paper to evaluate the system under various configurations.

The dispersion penalty is qualitatively similar to that occurring in analog fiber links [6]. Therefore, it has been suggested that the penalty can be minimized by employing optical SSB intensity modulation instead of the conventional optical DSB intensity modulation [7]. Optical SSB intensity modulation techniques can be classified into the categories of: 1) filtering and 2) phase discrimination. Filtering schemes use an optical filter to suppress one of the sidebands, while transmitting the carrier and the other sideband [8], [9]. In the TS-ADC, however, the carrier frequency varies with time (chirped carrier) and, hence, traditional filtering techniques cannot be used. By contrast, the phased discrimination methods could be utilized. One method for achieving this is shown in Fig. 2, using a dual-electrode modulator driven with the in-phase and quadrature RF signals [10]. However, both in theory and practice, it is well known that attaining  $90^\circ$  phase shift over a broad bandwidth is difficult to achieve, and typical hybrid couplers used for this purpose exhibit residual amplitude and phase imbalance over a broad bandwidth [11]. This results in imperfect sideband suppression and will impact the performance of the TS-ADC system. Therefore, it is not clear whether an SSB-modulated time-stretch system will improve the time-bandwidth product of the TS-ADC in practice, particularly over a wide RF bandwidth.

This paper is organized as follows. Section II describes the physical model of the time-stretched system and quantifies the limits on its time-bandwidth product for both DSB and SSB-modulation configurations. In addition, it discussed the special case when the signal is passband and the associated special design. Section III describes the analysis of the SSB time-stretched technique and quantifies the sensitivity to amplitude and phase errors in the SSB modulator. The analysis shows that, fortuitously, the TS-ADC system is tolerant to unavoidable phase and amplitude imbalance in the SSB modulator, implying that optical SSB intensity modulation is a practical solution to extending the system's time-bandwidth product. In Section IV, we present the experimental demonstration of a time-stretched ADC with the SSB modulation. The experiments demonstrate 120-GSample/s real-time capture of a 20-GHz SSB-modulated microwave signal.

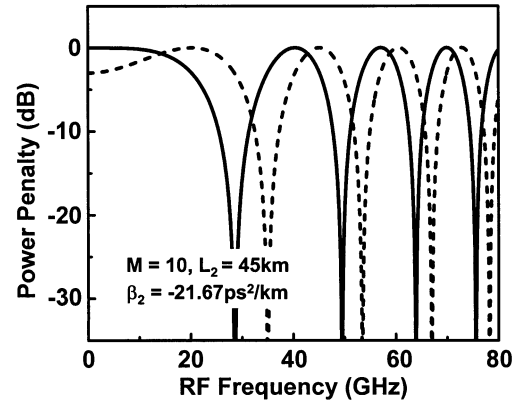


Fig. 3. Power penalty induced by fiber dispersion in time-stretched ADC using optical DSB intensity modulation. The solid line is for zero-chirp modulation and the dashed line is for chirped modulation.

## II. TIME-BANDWIDTH PRODUCT

The fundamental performance of the time-stretched system, shown in Fig. 2, is described by the following three expressions. The time aperture is given by  $T_A = 2\pi|\beta_2|\Delta f_{\text{op}}L_1$ , where  $\beta_2$  is the group velocity dispersion (GVD) parameter,  $L_1$  is the length of the first fiber used to provide wavelength-to-time mapping, and  $\Delta f_{\text{op}}$  is the optical bandwidth. The stretch factor is given by  $M = 1 + L_2/L_1$  [6], where  $L_2$  is the length of the second fiber. The dispersion penalty for the case of optical DSB intensity modulation that results from the interference between the carrier upper sideband and carrier lower sideband beat terms is given by [6]

$$H(f_{\text{rf}}) = \cos^2\left(\frac{4\pi^2 f_{\text{rf}}^2 \beta_2 L_2}{2M}\right) \approx \cos^2\left(\frac{4\pi^2 f_{\text{rf}}^2 \beta_2 L_1}{2}\right) \quad (1)$$

for  $M \gg 1$  and is plotted in Fig. 3 (solid line) where the zero-chirp or push-pull Mach-Zehnder (MZ) modulator biased at the quadrature point is assumed.

Naturally, it is highly desirable to maximize the time-aperture  $T_A$ . For a fixed optical bandwidth, it is possible to do so and maintain a constant stretch factor by increasing  $L_1$  while keeping the  $L_2/L_1$  ratio constant. However, a larger  $L_1$  increases the dispersion penalty and reduces the RF bandwidth. This tradeoff renders neither the time aperture, nor the bandwidth capable of assessing the performance, alone.

The amount of information contained in one segment is proportional to the ratio of the segment length (the time aperture)  $T_A$  and the maximum sample interval  $T_s$ . The Nyquist sampling theorem relates the maximum sample interval or equivalently minimum sampling frequency  $f_s = 1/T_s$  to the maximum RF bandwidth. In particular, it requires the sampling rate to be at least twice the RF bandwidth, or  $f_s \geq 2\Delta f_{\text{rf}}$ . Assuming sampling at the Nyquist rate ( $f_s = 2\Delta f_{\text{rf}}$ ), the ratio  $T_A/T_s$  is twice the direct product of the time aperture and RF bandwidth. For a passband signal, Nyquist theorem requires that  $f_s \geq 2\Delta f_{\text{rf}}(1 + f_L/\Delta f_{\text{rf}})/[1 + \text{Int}(f_L/\Delta f_{\text{rf}})]$ , where  $f_L$  is the lowest frequency of the passband signal and  $\text{Int}(x)$  is the integer part of  $x$ . For a wide-band signal, this expression reduces to  $f_s \geq 2\Delta f_{\text{rf}}$ .

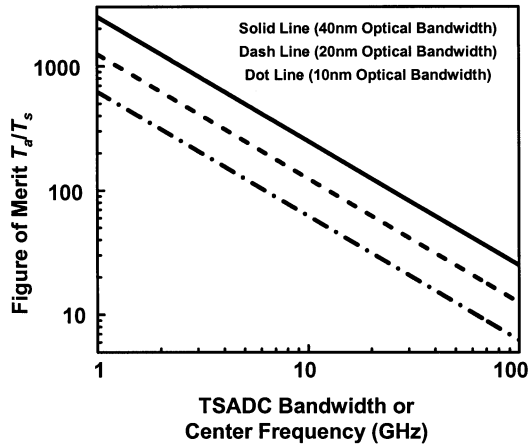


Fig. 4. Maximum achievable time-bandwidth product for a given 3-dB bandwidth (in the case of a baseband signal) or center frequency (in the case of a passband signal) in a DSB modulated time-stretched ADC. Zero-chirp modulation using a push-pull MZ modulator is assumed.

#### A. Time-Bandwidth Product for Optical DSB Intensity Modulation (Baseband Signal)

From (1), the 3-dB baseband bandwidth of the time-stretched preprocessor is equal to  $\Delta f_{\text{rf}} = [1/(8\pi|\beta_2|L_1)]^{1/2}$  for  $M \gg 1$ . Using this equation and the definition of time-aperture  $T_A$ , the time-bandwidth product of the baseband DSB modulation system can be obtained as follows:

$$\text{TBP}_{\text{DSB-BB}} \equiv \frac{T_A}{T_s} = 2T_A \Delta f_{\text{rf}} = \frac{\Delta f_{\text{op}}}{2\Delta f_{\text{rf}}}. \quad (2)$$

In (2), the time-bandwidth product only depends on the ratio of the optical-to-electrical bandwidth. Fig. 4 shows the calculated time-bandwidth product for a center wavelength of  $1.55 \mu\text{m}$  and supercontinuum bandwidths of 10, 20, and 40 nm, respectively. Clearly, there is a limit on the achievable time-bandwidth product for a given RF bandwidth.

The above results were obtained for a zero-chirp modulation achievable in a push-pull MZ modulator. The time-bandwidth product could be higher when chirped modulation is employed. When the chirp is opposite to that introduced by fiber dispersion, the dispersion penalty can be mitigated. Chirped modulation can be achieved using a single-arm MZ modulator biased at the quadrature point. In this case, (1) is modified to

$$H(f_{\text{rf}}) = \cos^2 \left( \frac{4\pi^2 f_{\text{rf}}^2 \beta_2 L_2}{2M} \pm \frac{\pi}{4} \right) \quad (3)$$

where the sign depends on the polarity of the bias. When the sign of the first term is opposite to the second term, the 3-dB bandwidth of baseband system is equal to  $\Delta f_{\text{rf}} = [1/(4\pi|\beta_2|L_1)]^{1/2}$  for  $M \gg 1$ , which is 41.4% larger than the zero-chirp case described above [12]. Hence, the time-bandwidth product could be 41.4% larger if chirped modulation with proper bias is used instead of zero-chirp modulation. The bandwidth enhancement is shown by the dashed line in Fig. 3, where the same electrical drive power was assumed for both the zero-chirp and chirped-modulation cases. There still exists limitation on the time-bandwidth product for a given bandwidth.

Equation (2) indicates that a larger optical bandwidth is required to obtain a larger time-bandwidth product in the DSB

modulated system. In practice, the maximum supercontinuum bandwidth that can be used will depend on the wavelength response of the optical modulator. For example, in a MZ modulator, deviation from the center wavelength results in a bias shift away from the quadrature point and a concomitant increase in second-order distortion [13]. In the multioctave system, this effect can limit the spurious-free dynamic range (SFDR). As an example, for an SFDR = 80 dB, the optical bandwidth is approximately 24 nm for an internally biased modulator [13]. By properly choosing the physical path length mismatch and external bias, the first-order wavelength dependence of the modulator can be eliminated, removing the limitation on the optical bandwidth [13]. The wavelength dependence of the photodetector response is of lesser concern, as it can be accurately characterized and calibrated.

#### B. Time-Bandwidth Product for Optical DSB Intensity Modulation (Passband Signal)

Referring to Fig. 3, for passband RF signals, one may be able to operate at one of the high-frequency lobes of the transfer function. In the passband operation, a longer  $L_1$  could be used, while maintaining a low-dispersion penalty and, hence, the time aperture of the system could be increased. However, this comes at the expense of RF bandwidth. According to (1), the carrier frequency corresponding to the peak of the  $n$ th sidelobe is  $f_{c,n} = [n/(2\pi|\beta_2|L_1)]^{1/2}$  for  $M \gg 1$ . The 3-dB bandwidth of this lobe is

$$\Delta f_{\text{DSB-PB}} = \left( \frac{n + \frac{1}{4}}{2\pi\beta_2 L_1} \right)^{(1/2)} - \left( \frac{n - \frac{1}{4}}{2\pi\beta_2 L_1} \right)^{(1/2)} \approx \frac{f_{c,n}}{4n} \quad (4)$$

for  $M \gg 1$ . Using this equation and the definition of time-aperture  $T_A$ , the time-bandwidth product of the DSB modulated system for the passband signal can be obtained as follows:

$$\text{TBP}_{\text{DSB-PB}} = \frac{T_A}{T_s} = 2T_A \Delta f_{\text{DSB-PB}} = \frac{\Delta f_{\text{op}}}{2f_{c,n}} \quad (5)$$

where the minimum passband sampling frequency  $f_s = 1/T_s$  is assumed to be  $2\Delta f_{\text{DSB-PB}}$ . This result is similar to that for the baseband signal case, except that the carrier frequency of the passband signal replaces the bandwidth of the baseband signal. With this in mind, the characteristics will be the same as that shown in Fig. 4. The passband scheme does not render a larger time-bandwidth product because the larger time aperture comes at the cost of proportionally reduced 3-dB bandwidth.

#### C. Time-Bandwidth Product for Optical SSB Intensity Modulation

The optical carrier is present in both SSB and DSB optical intensity modulation. The photodetector, being a square-law device, produces beating of various tones present in the optical domain. The penalty described by (1) arises due to dispersion-induced destructive interference between the carrier-sideband beat terms related to two sidebands in a DSB modulated signal. The beating occurs due to the square-law nature of the intensity photodetector. The process described

by (1) is similar to the dispersion penalty observed in RF fiber-optic links although, for a given fiber length, its magnitude is less due to the stretch process [6]. Recognizing this similarity, optical SSB intensity modulation can be employed for mitigating the dispersion penalty in the TS-ADC system [7]. In the context of the time-bandwidth product, SSB modulation eliminates the tradeoff between the large time aperture and the large bandwidth. The length of fiber  $l$  or, equivalently, the time aperture, could then be freely optimized without sacrificing the RF bandwidth if a broad-band SSB-modulation scheme is achievable. We note that, for the SSB case, a nonlinear phase distortion is present in the output waveform [7]. However, this can be removed in the digital domain using the known dispersion behavior of the fiber. This process is facilitated by the fact that since interference of the sidebands is avoided, signal power at the ADC input is preserved.

With SSB modulation, fiber dispersion will no longer limit the system bandwidth. Instead, the bandwidth of components, such as the RF hybrid coupler, will become important. In general, since the bandwidth limit is alleviated in SSB modulation, propagation loss of the fiber may become the dominant limit to the time-bandwidth product. The loss is proportional to the fiber length and, hence, will be proportional to the total amount of dispersion needed in the system. From the definition of the time-bandwidth product, the total amount of dispersion that is required to obtain a given stretch factor, time-bandwidth product, and RF bandwidth is given by

$$DL \approx \frac{M \cdot \text{TBP}}{2\Delta\lambda \cdot \Delta f_{\text{rf}}} \quad (6)$$

for  $M \gg 1$ , where  $D = (-2\pi c/\lambda^2)\beta_2$  is the dispersion coefficient and  $L = L_1 + L_2$ . As an example, for a stretch factor  $M = 10$ ,  $\Delta f_{\text{rf}} = 50$  GHz,  $\Delta\lambda = 40$  nm, and  $\text{TBP} = 1000$ , the total required dispersion is  $DL = 2500$  ps/nm. If standard single-mode fiber (SMF28) is used ( $DL = 17$  ps/km/nm, loss = 0.2 dB/km), there will be a total loss of 29.4 dB. A better performance can be obtained if the dispersion compensating fiber (DCF) is used ( $D = -90$  ps/km/nm, loss = 0.6 dB/km). With the DCF fiber, the loss is reduced to 16.7 dB. The relation between the time-bandwidth product and fiber loss is shown in Fig. 5.

We have shown that the dispersion penalty limits the capability of a DSB-modulated TS-ADC system by creating a tradeoff between the time aperture and RF bandwidth. A single-channel system with DSB modulation will be limited to a time-bandwidth product of approximately 100 for a bandwidth around 10 GHz. For the passband signal, operation at one of the high-frequency lobes of the system transfer function offers a larger time aperture, but at the expense of RF bandwidth. Hence, it does not offer any advantage in terms of the time-bandwidth product. SSB modulation removes the tradeoff between the time aperture and RF bandwidth, thus offering the potential to obtain a large time-bandwidth product. However, the following two practical challenges will have to be dealt with. First, as predicted by (6), the total fiber loss (proportional to  $L$ ) is proportional to the time-bandwidth product.

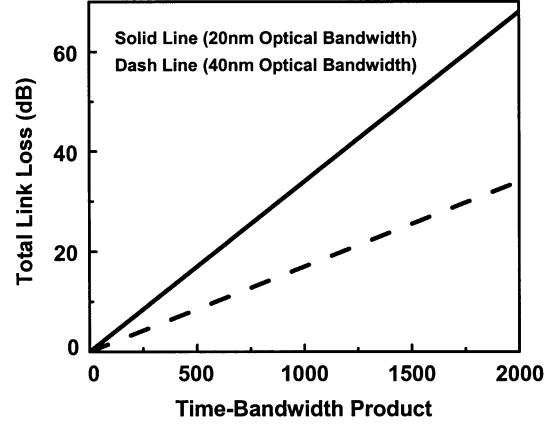


Fig. 5. Total fiber loss for a given time-bandwidth product in an optical SSB-modulated time-stretched ADC.  $M = 10$ ,  $f_{\text{rf}} = 50$  GHz. The DCF is assumed.

This will create a tradeoff between the signal-to-noise ratio (SNR) and time-bandwidth product. From this point-of-view, dispersive devices with superior dispersion-to-loss ratio than that obtainable with the DCF will be required. Additionally, proper design of an amplified photonic time-stretched system is important. The second practical challenge is the ability to perform SSB modulation over a large RF bandwidth. Since the optical carrier in the time-stretched system is broad-band, traditional filtering techniques for SSB modulation cannot be used. Phase-discrimination methods for SSB modulation require a  $90^\circ$  phase shifter that is normally not ideal and has a limited bandwidth and lack accuracy. This practical issue is discussed in Section III.

### III. ANALYSIS OF SSB-MODULATED TIME-STRETCHED SYSTEM

As discussed in the previous sections, in the DSB-modulated TS-ADC system, the dispersion penalty results in a frequency-dependent attenuation in the electrical domain, which arises due to destructive interference between the two carrier-sideband beat terms in the photodetector. Hence, SSB modulation is a potential solution. The quality of SSB modulation can be quantified by the sideband rejection ratio, which is defined in this paper as the ratio of amplitudes of the two sidebands. Assuming that the SSB modulator shown in Fig. 2 is used, the output optical field  $E_{\text{out}}(t)$  could be related to the input optical field  $E_{\text{in}}(t)$  by

$$E_{\text{out}}(t) = \frac{E_{\text{in}}(t)}{2} \left\{ \exp \left[ i \left( \frac{\pi}{2} + \frac{m}{2} \cos \omega_{\text{rf}} t \right) \right] + \exp \left[ i \frac{r m}{2} \sin(\omega_{\text{rf}} t + \Delta\phi) \right] \right\} \quad (7)$$

where the modulator is biased at the quadrature point.  $\omega_{\text{RF}}$  is the RF angular frequency and  $m$  is the optical modulation index defined as  $m = \pi V_{\text{rf}}/V_{\pi}$ , in which  $V_{\text{rf}}$  and  $V_{\pi}$  are the RF voltage amplitude and the half-wave voltage, respectively.  $r$  is the inter-electrode signal-amplitude ratio (ideally equal to unity), and  $\Delta\phi$  is the deviation of inter-electrode phase difference from  $90^\circ$ .

The quality of the hybrid coupler and symmetry of the dual-electrode modulator are the main factors that determined  $r$  and  $\Delta\phi$ . Invoking the Bessel function expansion, (7) can be written as

$$E_{\text{out}}(t) = \frac{E_{\text{in}}(t)}{2} \sum_{n=-\infty}^{\infty} \left[ J_n\left(\frac{m}{2}\right) i^{n+1} + J_n\left(\frac{rm}{2}\right) \cdot \exp(in\Delta\phi) \right] \exp(in\omega_{\text{rf}}t) \quad (8)$$

The sideband field suppression ratio  $R$  can then be obtained as follows:

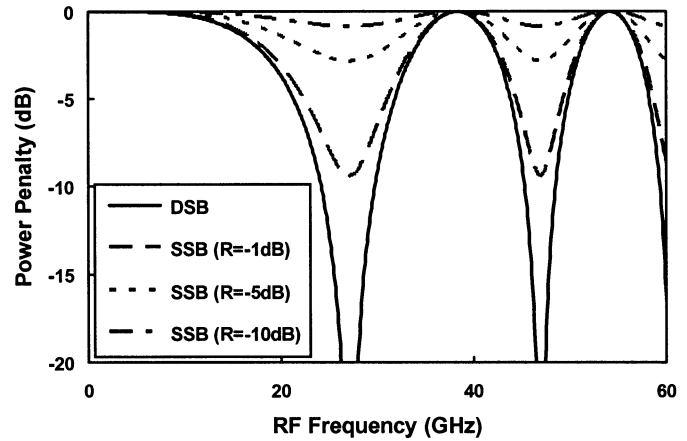
$$R = \frac{\left| J_1\left(\frac{rm}{2}\right) \exp(i\Delta\phi) - J_1\left(\frac{m}{2}\right) \right|}{\left| J_1\left(\frac{rm}{2}\right) \exp(-i\Delta\phi) + J_1\left(\frac{m}{2}\right) \right|} \approx \frac{\left| r \exp(i\Delta\phi) - 1 \right|}{\left| r \exp(-i\Delta\phi) + 1 \right|} \quad (9)$$

where the approximation is valid when the modulation index  $m$  is small. Equation (9) shows that, for small modulation depths,  $R$  is independent of the modulation depth and depends only on the phase and amplitude imbalances between two arms. Over its operating bandwidth, typical imbalance parameters for a commercially available hybrid coupler are  $r = \pm 0.6$  dB and  $\Delta\phi = \pm 7^\circ$ .<sup>1</sup> Substituting these values into (9), we obtain  $R = -10.4$  dB.

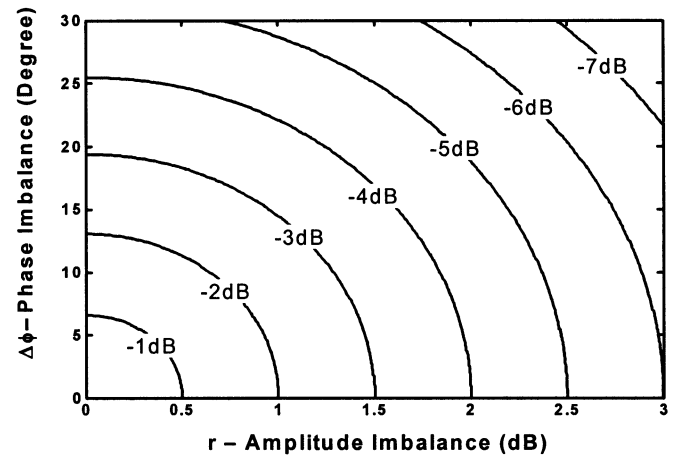
The interference between the two sideband-carrier beat signals results in the photodetector current of the form  $I(t) \propto \cos(\omega_{\text{rf}}t - \phi_{\text{DIP}}) + R \cos(\omega_{\text{rf}}t + \phi_{\text{DIP}})$ , where  $\phi_{\text{DIP}} = (1/2)\beta_2(L_2/M)\omega_{\text{rf}}^2$  [6]. For the DSB modulated system, where  $R = 1$ , it is reduced to the dispersion penalty equation, which suggests that the RF power is scaled by  $\cos^2 \phi_{\text{DIP}}$  [6]. More generally, the power transfer function will depend on  $R$  and is given by

$$H = \left( \frac{1-R}{1+R} \right)^2 \sin^2 \phi_{\text{DIP}} + \cos^2 \phi_{\text{DIP}}. \quad (10)$$

When  $\phi_{\text{DIP}} = \pi/2$ , dispersion penalty reaches its maximum value  $[(1-R)/(1+R)]^2$ . Fig. 6(a) shows the dispersion penalty for different sideband amplitude suppression ratios for a system with  $L_2 = 50$  km and  $M = 10$ . It is evident that even a modest SSB suppression greatly reduces the dispersion penalty. As an example, when  $R = -10.4$  dB, the maximum power penalty is 1.6 dB, which is acceptable for most applications. To show the sensitivity of the dispersion penalty to physical parameters, the contour plot in Fig. 6(b) shows the maximum power penalty as a function of amplitude and phase imbalances in the dual-arm SSB modulator (Fig. 2). As can be observed, to obtain a power penalty of less than 3 dB, the maximum amplitude imbalance of 1.5 dB, or a maximum phase imbalance of  $19^\circ$  can be tolerated. This information is of critical importance in the physical design of the SSB-modulated TS-ADC system. Further, with  $M = 1$ , the expression for the dispersion-induced-phase term  $\phi_{\text{DIP}}$  reduces to the same for an analog optical link of length  $L_2$ . Therefore, the analytical model developed here is equally applicable



(a)



(b)

Fig. 6. (a) Dispersion penalty curves for DSB modulation and SSB modulation with different sideband suppression ratios  $R$ . (b) Contour map of maximum dispersion penalty (marker values) as a function of amplitude and phase imbalances in the SSB modulator.

to RF fiber-optical links with the same modulation scheme and layouts as the basic design framework.

#### IV. EXPERIMENTS

To investigate the performance of the SSB-modulation scheme used in the TS-ADC (Fig. 2), an external-cavity diode laser was used as the carrier so that the modulation sidebands can be examined directly in the optical spectrum analyzer. The typical modulated optical spectrum is shown in Fig. 7(a). Fig. 7(b) shows the sideband power suppression ratio (SPSR) obtained from the measured optical spectrum. Results show that a minimum suppression of  $-18.8$  dB is achieved across the 8–18-GHz bandwidth. Based on the worst case amplitude and phase imbalances of the hybrid coupler (0.6 dB and  $7^\circ$  across 4–18 GHz), we calculate a  $\text{SPSR} = R^2 = -20.8$  dB. The difference between this and the measured value can be attributed to the imbalance in the modulator, which is not considered in the theoretical value.

Also shown in Fig. 7(b) is the maximum dispersion penalty corresponding to the measured SPSR based on (10). Results indicate that the penalty can be kept to less than 2.5 dB from 8 to 20 GHz. The lowest frequency that could be measured

<sup>1</sup>Anaren Microwave Inc., East Syracuse, NY, 90° hybrid coupler (model 10029-3). [Online]. Available: [http://www.anaren.com/products/product\\_detail.cfm?prod=611](http://www.anaren.com/products/product_detail.cfm?prod=611)

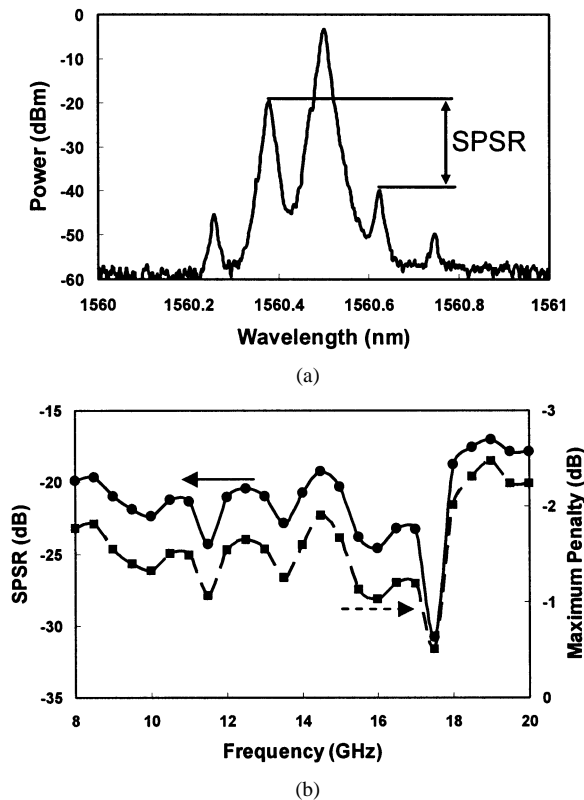


Fig. 7. (a) Measured optical spectrum of the SSB-modulated signal. The SPSR denotes sideband power suppression ratio. (b) Measured frequency dependence of the SPSR (solid line) and the corresponding maximum power penalty (dash line).

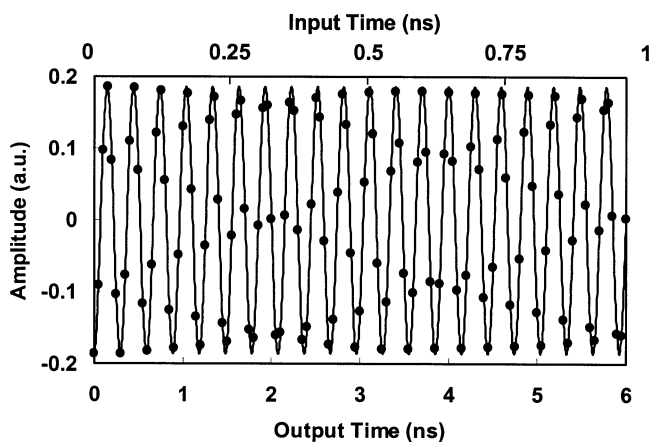


Fig. 8. 120-GSamples/s real-time capture of a 20-GHz RF signal by the SSB TS-ADC system. Measured data (symbols) and fitted sine curve (solid line) of a time-stretched ADC.

was limited to 8 GHz by optical spectrum analyzer. However, since the hybrid coupler maintains the specified amplitude and phase imbalance down to 4 GHz, we conclude that the maximum penalty will be 2.5 dB across 4–20 GHz.

Fig. 8 shows the 20-GHz signal captured at 120 GSamples/s with the SSB TS-ADC. The noise bandwidth was limited to 4 GHz around 20 GHz. The DCF was used as the dispersive element. The stretch factor is measured to be 5.94, the optical modulation index is 18.6%, and the input aperture is 2.9 ns. The electronic ADC is the Tektronix TDS7404 digital oscilloscope with

4-GHz input bandwidth and a 20-GSa/s sample rate. Therefore, the effective input sample rate is approximately 120 GSamples/s.

One of the challenges in the TS-ADC system is the nonuniform spectral density of the supercontinuum source and its pulse-to-pulse variation. The flatness is determined primarily by that of the source, as well as the influence from optical filters and the erbium-doped fiber amplifier gain profile. Owing to the wavelength-to-time mapping occurring in the first fiber, spectral nonuniformities appear as a temporal modulation of the chirped-carrier amplitude entering the modulator. As long as the variation is slow compared to the RF input signal, it can be separated from the signal (by low-pass filtering) and used for correction. This method will place a low-frequency cutoff on the system, but otherwise, is highly effective for compensating for the spectral nonuniformity and its pulse-to-pulse dependence. It was employed in the above experiments.

## V. SUMMARY

In summary, we have defined the time-bandwidth product as the proper metric to evaluate the performance of the photonic time-stretched ADC, and have used it to compare DSB and SSB optical modulation schemes. It was shown that there exists a tradeoff between the RF bandwidth and time aperture of the system in the DSB modulated system. This tradeoff arises due to the dispersion penalty in the system and is qualitatively similar to that in conventional analog fiber-optic links. The penalty results in attenuation of high-frequency components and is a manifestation of DSB modulation. Therefore, SSB modulation is a natural choice for removing the bandwidth limitation and for maximizing the time-bandwidth product. Theoretically, with SSB modulation, there is no fundamental limit to system bandwidth, aside from component limitations (i.e., the SSB modulator and photodetector). The system will then be loss limited, and a time-bandwidth product of around 1000 is readily achievable. While a phase distortion is present in the SSB time-stretched waveform, it can be corrected in the digital domain using the known dispersion characteristic of the fiber.

Since the optical carrier in the time-stretched system has a broad optical bandwidth and is chirped, filtering techniques cannot be used for SSB generation, and phase discrimination using a dual-arm MZ modulator is the only viable approach. In practice, the maximum bandwidth of these systems is limited by the phase and amplitude imbalance in the hybrid RF coupler used to create quadrature signal components. Our analytical results indicate that, fortuitously, the TS-ADC system is tolerant to such errors. The analytical results developed here are equally applicable to conventional RF fiber-optic links. Experiments using commercially available components showed that the dispersion-induced power penalty can be kept below 2.5 dB over a 4–20 GHz bandwidth for any stretch factor. In further experiments, SSB-modulated time stretch was used to digitize a 20-GHz RF tone with 4-GHz input bandwidth at 120 GSamples/s using a 20-GSamples/s electronic digitizer.

## ACKNOWLEDGMENT

The authors would like to thank Dr. J. Murphy, Defense Advanced Research Projects Agency (DARPA), and Dr. R. Leheny,

DARPA, for their support. The authors would also like to acknowledge helpful discussions with J. Han, University of California at Los Angeles (UCLA), and Prof. H. Fetterman, UCLA.

#### REFERENCES

- [1] B. Jalali and F. Coppinger, "Data conversion using time manipulation," U. S. Patent 6288 659, Sept. 11, 2001.
- [2] B. Asuri, Y. Han, and B. Jalali, "Time-stretched ADC arrays," *IEEE Trans. Circuits Syst. II*, vol. 49, pp. 521–524, July 2002.
- [3] W. C. Black and D. A. Hodges, "Time interleaved converter arrays," *IEEE J. Solid-State Circuits*, vol. SC-15, pp. 1022–1029, Dec. 1980.
- [4] A. S. Bhushan, P. V. Kelkar, B. Jalali, O. Boyraz, and M. Islam, "130 GSa/s photonic analog-to-digital converter with time-stretched preprocessor," *IEEE Photon. Technol. Lett.*, vol. 14, pp. 684–686, May 2002.
- [5] O. Boyraz, J. Kim, M. N. Islam, F. Coppinger, and B. Jalali, "10 Gb/s multiple wavelength, coherent short pulse source based on spectral carving of supercontinuum generated in fibers," *J. Lightwave Technol.*, vol. 18, pp. 2167–2175, Dec. 2000.
- [6] F. Coppinger, A. S. Bhushan, and B. Jalali, "Photonic time-stretched and its application to analog-to-digital conversion," *IEEE Trans. Microwave Theory Tech.*, vol. 47, pp. 1309–1314, July 1999.
- [7] J. M. Fuster, D. Novak, A. Nirmalathas, and J. Marti, "Single sideband modulation in photonic time-stretched analogue-to-digital conversion," *Electron. Lett.*, vol. 37, pp. 67–68, 2001.
- [8] K. Yonenaga and N. Takachio, "A fiber chromatic dispersion compensation technique with an optical SSB transmission in optical homodyne detection systems," *IEEE Photon. Technol. Lett.*, vol. 5, pp. 949–951, Aug. 1993.
- [9] J. Park, W. V. Sorin, and K. Y. Lau, "Elimination of the fiber chromatic dispersion penalty on 1550 nm millimeter-wave optical transmission," *Electron. Lett.*, vol. 33, no. 6, pp. 512–513, 1997.
- [10] G. H. Smith, D. Novak, and Z. Ahmed, "Technique for optical SSB generation to overcome dispersion penalties in fiber-radio systems," *Electron. Lett.*, vol. 33, pp. 74–75, 1997.
- [11] K. Chang, I. Bahl, and V. Nair, *RF and Microwave Circuit and Component Design for Wireless Systems*. New York: Wiley, 2002, ch. 6.
- [12] J. Han, B.-J. Seo, Y. Han, and H. R. Fetterman, "Photonic time-stretching system using polymer SSB modulators," presented at the IEEE Lasers and Electro-Optics Conf., 2003.
- [13] S. Dubovitsky, W. H. Steier, S. Yegnanarayanan, and B. Jalali, "Analysis and improvement of Mach-Zehnder modulator linearity performance for chirped and tunable optical carriers," *J. Lightwave Technol.*, vol. 20, pp. 858–863, May 2002.



**Yan Han** received the B.S. and M.S. degrees in electronic engineering from the Tsinghua University, Beijing, China in 1998 and 2000, respectively, and is currently working toward the Ph.D. degree in electrical engineering at the University of California at Los Angeles (UCLA).

His research interests include the areas of microwave photonic systems, optical communication systems, wireless communication systems, optical amplifiers, and fiber optics.



**Bahram Jalali** (S'86–M'87–SM'97) is currently a Professor of electrical engineering, the Director of the Defense Advanced Research Projects Agency (DARPA) Center for Optical A/D System Technology (COAST), and the Director of the Optoelectronic Circuits and System Laboratory, University of California at Los Angeles (UCLA). From 1988 to 1992, he was a Member of Technical Staff with the Physics Research Division, AT&T Bell Laboratories, Murray Hill, N.J. where he conducted research on ultrafast electronics and optoelectronics.

He was responsible for successful development and delivery of 10-Gb/s lightwave circuits to the U.S. Air Force in 1992. While on leave from UCLA from 1999 to 2001, he founded the fiber-optic component company Cognet Microsystems, Los Angeles, CA. He served as Cognet's CEO, President and Chairman, from the company's inception through its acquisition by Intel Corporation in April 2001. He currently serves as Chief Scientist with the Optical Component Division, Intel Corporation, in addition to his faculty position at UCLA. He has authored or coauthored over 130 publications. He holds five U.S. patents. His current research interests are microwave photonics, integrated optics, and fiber optic integrated circuits.

Dr. Jalali is a member of the California Nano Systems Institute (CNSI) and is the chair of the Los Angeles Chapter of the IEEE Lasers and Electro-Optics Society (IEEE LEOS). He was the general chair for the IEEE International Conference on Microwave Photonics (MWP) in 2001 and its Steering Committee chair from since 2001. He serves on the Board of Trustees of the California Science Center. He was the recipient of the BridgeGate 20 Award in recognition of his contributions to the Southern California hi-tech economy.